Fernández-Duque, B., Pérez, I. A., Sánchez, M. L., García, M. Á., & Pardo, N. (2017). Temporal patterns of CO 2 and CH 4 in a rural area in northern Spain described by a harmonic equation over 2010–2016. *The Science of the Total Environment,* 593-594, 1-9. https://doi.org/10.1016/j.scitotenv.2017.03.132

Temporal patterns of CO_2 and CH_4 in a rural area in northern Spain described by a harmonic equation over 2010-2016

Beatriz Fernández-Duque, Isidro A. Pérez*, M. Luisa Sánchez, M. Ángeles García and Nuria Pardo

Department of Applied Physics

Faculty of Sciences

University of Valladolid

Paseo de Belén, 7

47011 Valladolid, Spain

*Corresponding author

Phone: 34 983 184 189

Fax: 34 983 423 013

e-mail: iaperez@fa1.uva.es

Abstract

The present paper seeks to improve our knowledge concerning the evolution of CO_2 and CH_4 in terms of monthly trends, growth rate and seasonal variations in the lower atmosphere. Dry continuous measurements of CO_2 and the CH_4 mixing ratio were carried out over five and a half years (from 15 October 2010 to 29 February 2016) by multi-point sampling at 1.8, 3.7 and 8.3 m, using a Picarro analyzer at a rural site in the Low Atmosphere Research Centre (CIBA), on the upper Spanish plateau. Data were divided into diurnal and nocturnal records. The mathematical equation proposed to analyze the overall data was a harmonic one, comprising a polynomial (trend) and a series of harmonics (seasonal cycle). Amplitude was considered as a constant and variable term over time. Quite different behaviour was found between day and night measurements in both climate forcing agents. CO_2 showed an accelerating trend in autumn, whereas CH_4 trends were higher during the winter. Increasing growth rates were reported for CO_2 and CH_4 over the whole study period. Nocturnal CO_2 amplitudes are higher than diurnal ones except in winter for both gases, and also in the autumn for CH_4.

Key words: upper Spanish plateau, greenhouse gases, series of harmonics, daytime, night-time.

1. Introduction

Two of the major trace constituents warming the planet are carbon dioxide (CO_2) and methane (CH_4), commonly known as "greenhouse gases" (GHGs). Any change in the atmospheric amount of greenhouse gases results in the redistribution of the energy in the atmosphere surface system and leads to a change in surface temperature, contributing to global climate change, and posing one of the major challenges facing humankind today (Haszpra et al., 2008). The contribution of radiative forcing from one CH_4 molecule is 25 times higher than CO_2 (Fang et al., 2013b). However, mean tropospheric lifetime is around 10 years for CH_4 and 30 for CO_2 (García et al., 2016).

Over the last ten years or so, fossil fuel combustion and industrial activities have been the major CO_2 sources yielding 9.3 ± 0.5 GtC year^{-1} (Global Carbon Project, 2016). Respiration processes from plants and soils (Sreenivas et al., 2016) as well as land use changes (Li et al., 2014) must also be considered. In contrast, the main CO_2 sinks for the same period of time, have been terrestrial ecosystems (3.1 ± 0.9 GtC year^{-1}) and oceans (2.6 ± 0.5 GtC year^{-1}) (Global Carbon Project, 2016).

As stated before, terrestrial ecosystems can act as important CO_2 sources or sinks. Plants mainly take carbon out of the atmosphere through photosynthesis in summer, thereby decreasing CO_2 concentrations, and release it in autumn and spring, thus increasing concentrations (Barlow et al., 2015). The type of ecosystem plays a very important role in this cycle, as well as, meteorological conditions (Fang et al., 2014).

Barlow et al. (2015) reported increases in the amplitude of seasonal exchange of CO_2 since the 1950s, particularly at mid-to high northern latitudes (Graven et al., 2013). CO_2 growth rates at different stations in the Northern Hemisphere have varied by around 1–3 ppm over the past decade (Huang et al., 2015).

As regards CH_4, it should be remembered that around 60-70% of emissions are from anthropogenic sources (Fang et al., 2013a; Haszpra et al., 2008), with approximately two thirds originating from the Northern Hemisphere as reported by Lelieveld (2006) (Sánchez et al., 2014). Anthropogenic CH_4 sources include fermentation in livestock and manure management (106 Tg $year^{-1}$), gas (79 Tg $year^{-1}$), landfills and waste water treatment (59 Tg $year^{-1}$), coal mining (42 Tg $year^{-1}$) and biomass burning (30 Tg $year^{-1}$) when incomplete combustion occurs (Global Carbon Project, 2016; Haszpra et al., 2008; Sánchez et al., 2014). The main natural CH_4 sources are principally wetlands (185 Tg $year^{-1}$), followed by peatlands, wild animals, digestion processes in termites, microorganisms living in the oceans, forest fires, CH_4 carbohydrates and permafrost (García et al., 2016; Global Carbon Project, 2016; Sánchez et al., 2014).

On the other hand, oxidation of this gas by OH radicals in the troposphere is the major sink and accounts for 90% of CH_4 loss in the atmosphere (Fang et al., 2013a). Due to the photochemical nature of OH radicals, reactions are particularly enhanced in summer (Sánchez et al., 2014). Therefore, a maximum in the OH sink drives the summer minima in CH_4 (Buchholz et al., 2016). Overlaid on the cycle induced by OH is the seasonality of source contributions (Buchholz et al., 2016). Topp and Pattey (1997) point to microbial uptake by soils and reactions in the stratosphere as other sinks (Sánchez et al., 2014).

Global atmospheric CH_4 mole fractions went unnoticed from 1999 to 2006 (increasing by 6 ppb) and then increased rapidly from 2007 to 2011 (29 ppb) (Fang et al., 2013a). The reasons for the new increase are not yet perfectly understood (Fang et al., 2013a). The insufficient number of monitoring stations, especially in rural areas, is one of the reasons underlying this lack of understanding (Sánchez et al., 2005).

69 The main goal of the present study is to quantify the baseline concentration and
70 interpret the results regarding the ecosystem and atmospheric behaviour in terms of
71 annual cycle and inter-annual variability. To achieve this goal, a harmonic equation is
72 employed. The use of harmonic functions is not new in trace gases analyses. Nakazawa
73 et al. (1997) suggested that the trend of the data must be fitted by a polynomial term of
74 suitable degree, whereas the seasonal cycle may be described by a series of harmonic
75 terms. Anderson-Cook (2000) used a second harmonic model for cylindrical data
76 involving wind direction and temperature. Chamard et al. (2003) and Artuso et al.
77 (2009) employed a function consisting of an exponential term and two harmonics in line
78 with Fourier analyses. A fourth-order polynomial term with one harmonic was
79 developed by Inoue et al. (2006). Sánchez et al. (2008) employed one harmonic
80 function, considering the amplitude fixed and variable with time, to analyze the ozone
81 trend at the CIBA station for a six-year period. Sánchez et al. (2010) applied a model
82 comprising a linear polynomial term plus two harmonics, only one of which was
83 variable over time, expressing seasonality. Wu et al. (2012) and Liu et al. (2015) fitted
84 the data to a function with a linear polynomial and two harmonic functions considering
85 the variable term but in a simplified manner. Others, such as Fang et al. (2013b), have
86 used a quadratic polynomial plus the sum of four harmonics, without considering the
87 variable term.

88 In line with the previous literature, many authors have applied harmonic functions to
89 describe the behaviour of pollutants in the troposphere. However, researchers who have
90 employed four harmonics have not considered the amplitude variable over time for the
91 seasonal cycle, resulting in a worse fit of the data, since CO_2 and CH_4 concentrations
92 are time-dependent variables. Those who have developed a harmonic model in which
93 amplitude depends on time have not considered four harmonics, which involves a loss

of annual and interannual information in the cycle. For these reasons, this paper develops a function taking into account both considerations. Recorded data were fitted into a harmonic function, producing a prediction pattern for each instant that was the sum of a linear trend based on a third-degree polynomial plus four harmonics, each made up of a constant and a variable part along the time series. This enhancement provides a better data fit and gives more accurate results.

Previous studies on the measurement site have not considered the evolution of these gases, but analyzed the distributions of the observations (Pérez et al., 2013; 2014). This paper focuses on the differences between daytime and night-time, while other studies of this research group examined total observations without differentiating between daytime and night-time (Pérez et al., 2016; 2017). The findings of this study may improve current knowledge concerning the evolution of CO_2 and CH_4 in a rural area of Southern Europe over the last five years.

2. Materials and methods

2.1 Site description

Dry continuous atmospheric CO_2 and CH_4 measurements were carried out from 15 October 2010 to 29 February 2016 at the Low Atmosphere Research Centre (CIBA) in the centre of the upper Spanish plateau (lat: 41°48′49″N, long: 4°55′59″W, alt: 845 m). Figure 1 shows the location of the CIBA station and its surrounding area.

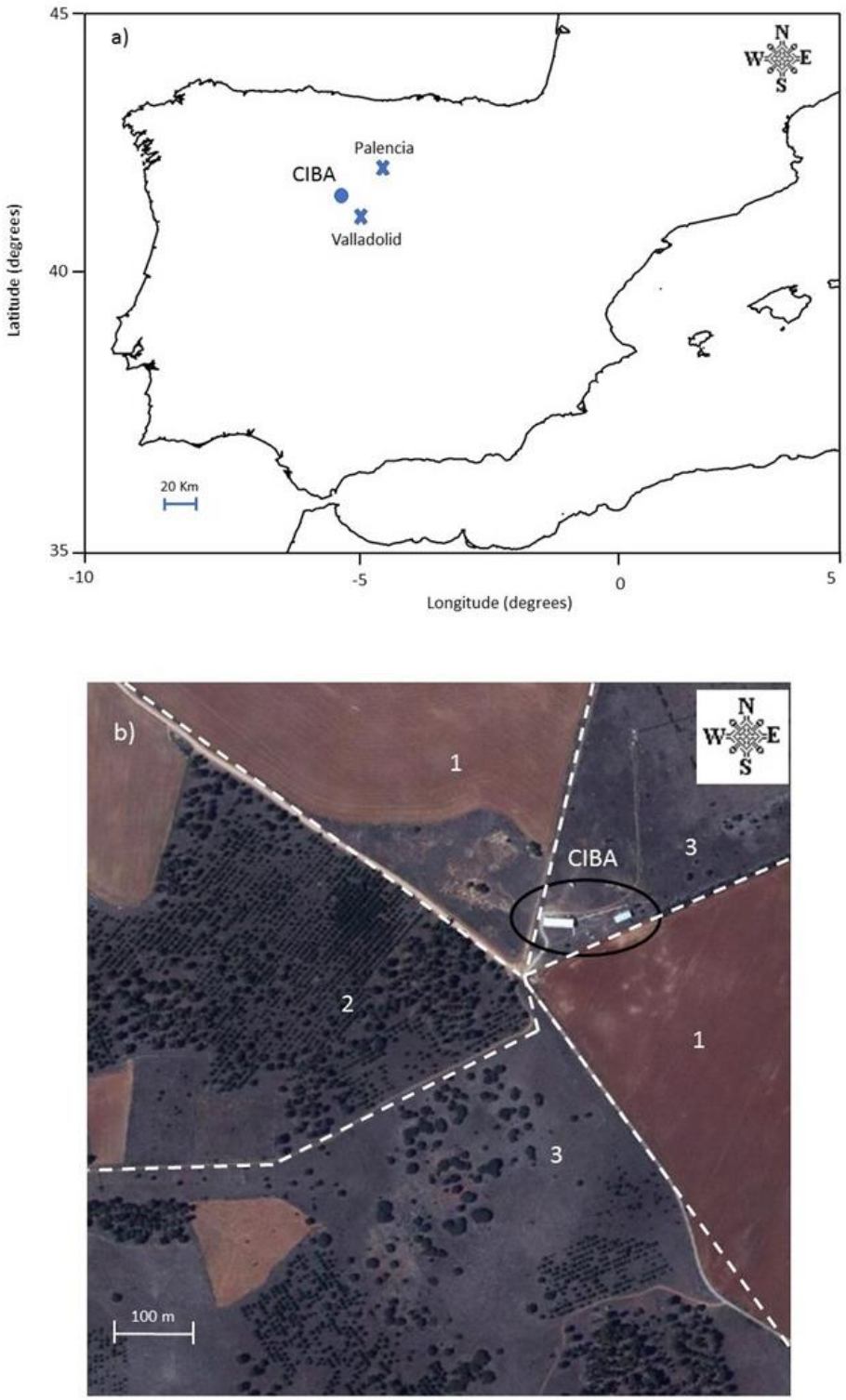

114

115 Fig.1. a) Location of the CIBA station on the upper Spanish plateau. b) PNOA image
116 courtesy of © ign.es showing the land use around the sampling site, surrounded by a
117 black line. Number 1 represents agricultural crops, 2 coniferous forest, and 3 a scrub-
118 grassland association.

The monitoring station is located in a rural area (Fig. 1a) away from major industrial sources. The closest largest cities are Valladolid (304,000 inhabitants) 24 km to the southeast and Palencia (80,000 inhabitants) 40 km to the northeast. The surrounding area (Fig. 1b) is characterized by non-irrigated crops and grass (Pérez et al., 2009a) and a small area of coniferous forest. There are no relief elements, such that horizontal homogeneity can be assumed (Pérez et al., 2009c).

The site is under a Mediterranean continental climate (García et al., 2012) with four distinct seasons. Maximum temperatures are recorded in summer, July-August, and minimum in winter, December-January (Sánchez et al., 2003). Annual precipitation in the centre of the plateau is around 450 mm (Sánchez et al., 2014), with an evenly distributed pattern throughout the year (García et al., 2012), peaking in autumn and spring (Sánchez et al., 2014).

2.2 Instrumentation

A high precision Cavity Ring-Down Spectroscopy (CRDS) analyzer (G1301, PICARRO Inc) is used for continuous atmospheric measurements at the CIBA station. The response presents high linearity with concentrations and the signal is very stable (Fang et al., 2014) and accurate and requires little maintenance (Sánchez et al., 2014). A detailed discussion of this instrument and the necessary calibration has been addressed by Buchholz et al. (2016) or Haszpra et al. (2008) among others.

The analyzer software includes a valve sequencer to automatically control external solenoid valves to measure at 1.8, 3.7 and 8.3 m (García et al., 2016).

2.3 Dataset

142 Data collection is mostly complete except for sporadic gaps caused by instrument
143 malfunction (e.g., stream selection valves shifted to a wrong position), calibration,
144 maintenance or power failure. Boundary layer height values at the CIBA station were
145 obtained by METeorological data EXplorer web-based systems (Zeng et al., 2010) for
146 the whole study period. To gain a better understanding of the atmospheric patterns
147 between day and night the overall series has been divided taking the GMT hour from
148 the National Geographic Institute of Spain as a reference. Concentrations were analyzed
149 based on semi-hourly means.

150 The Fisher method was applied to the dataset in order to study the statistical differences
151 between levels. Using this procedure, if the intervals of a pair of samples do not overlap
152 in the vertical direction, their means could be considered different.

153 *2.4 Mathematical expression*

154 To evaluate the global evolution of CO_2 and CH_4 mole fractions, a harmonic equation
155 has been applied, which can simultaneously separate the long-term trend and the
156 seasonal cycle while retaining information about changes in amplitude.

157 The fitted curve used in this paper may thus be written as follows:

158 $$y = \sum_{i=0}^{3} a_i t^i + \sum_{j=1}^{4} \sum_{k=0}^{1} \left(b_{jk}\, \mathrm{t}^{\mathrm{k}} \cos(j2\pi t) + c_{jk}\, \mathrm{t}^{\mathrm{k}} \sin(j2\pi t) \right) \qquad (1)$$

159 In the above expression, "*y*" represents the CO_2 or CH_4 mole fraction and time (*t*) is
160 expressed as a fraction of year based on the number of data between the start date (15
161 October 2010) and the end date (29 February 2016).

162 The unknown coefficients of the multiple harmonic regression were linearly estimated
163 running MATLAB© software. Independent variables were time (t, t^2, t^3) and the series of
164 harmonics $t^k\, cos(j2\pi t)$, $t^k\, sin(j2\pi t)$.

165 The polynomial supplies information about the data trend. A third-degree polynomial
166 has been considered since Nakazawa et al. (1997) did not specify the suitable degree
167 and other authors such as Fang et al. (2013b) and Inoue et al. (2006) have adopted
168 similar orders.

169 The sequence of four harmonics (j) provides information about the yearly cycle. As the
170 main goal of this paper is to describe baseline concentrations of both gases in terms of
171 annual cycle and inter-annual changes, we need to employ four harmonics. The two first
172 harmonics refer to annual behaviour. The first (j=1), expresses annual behaviour and the
173 second (j=2) reinforces this information, sharpening the peaks and troughs. The third
174 harmonic (j=3) refers to four month changes and the fourth (j=4) to quarterly
175 information, that is say, both harmonics give the seasonal evolution.

176 The main contribution of Eq (1) is to consider amplitude as a constant and a variable
177 term along the time series. As mentioned in the Introduction section, to the best of the
178 author's knowledge, the variable term has not been widely studied. Contributions of
179 other authors including Inoue et al. (2006) or Wu et al. (2012) have considered the
180 variable term but in a simple way. We strongly believe that a further evaluation of its
181 influence in the seasonal cycle is required. The term in which the amplitude is constant
182 with time represents the general features of the seasonal cycle. According to Sánchez et
183 al. (2010), this term explains around 87% of the seasonal cycle. However, the term in
184 which the amplitude is variable along the time series reinforces the information of the
185 fixed term, offering more accurate results and endowing the data with greater flexibility.
186 The index k reflects the term in which amplitude is constant with time ($k=0$) and the
187 other in which it is variable ($k=1$) over time.

188

3. Results and discussion

3.1. Measures at the three levels

We found no statistical differences between the three levels during daytime (Fig. 2) in line with Pérez et al. (2012a), due to thermal turbulence in the lower atmosphere, which causes an intensive vertical mixture as suggested by said author. Figure 2 reflects the least significant difference between samples in accordance with the Fisher method with a confidence interval of 95%.

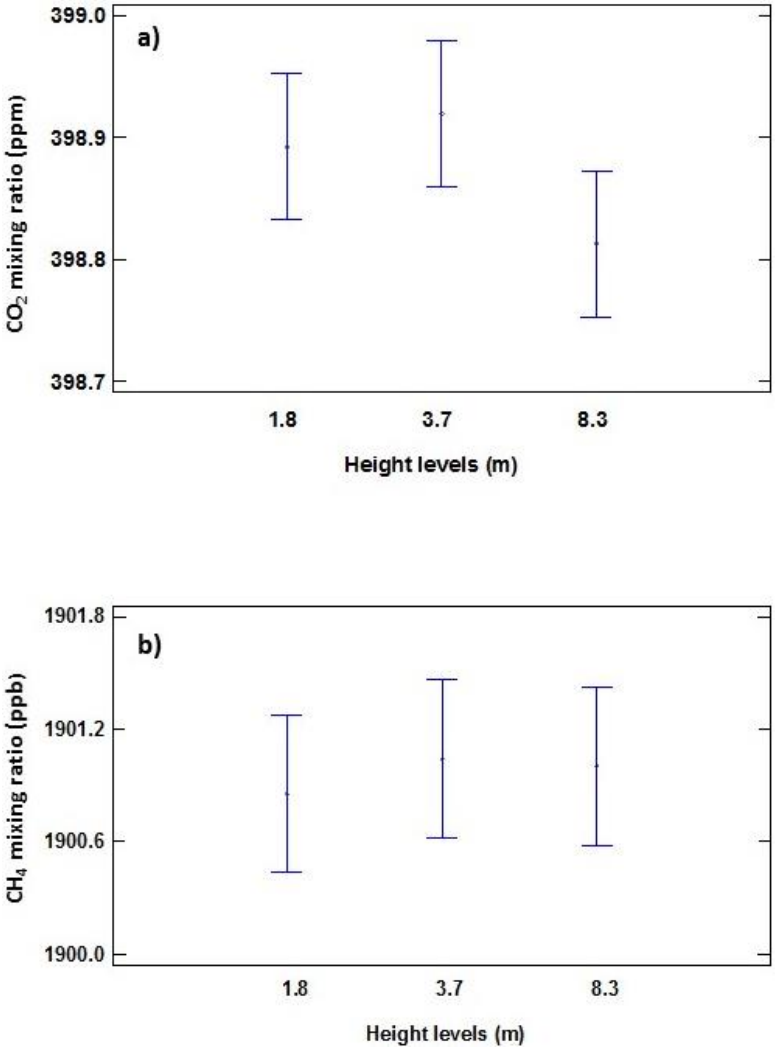

Fig. 2. Least significant difference (LSD) intervals for CO_2 and CH_4 mixing ratio during daytime for the three levels measured: a) CO_2 results. b) CH_4 results.

199 Controversially, we found small differences in the nocturnal data (Fig. 3) attributed to
200 vegetation respiration intensified by the stability increase, as suggested by Pérez et al.
201 (2012a). As the height of the measurement increases, the CO_2 concentration decreases
202 (Fig. 3a) as reported by other authors such as Fang et al. (2013a; 2014) and Lee et al.
203 (2012). This decrease may be due to the lower dispersion linked to lower wind speed as
204 reported by Pérez et al. (2012a). With regard to CH_4, concentrations grow as height
205 increases (Fig.3b), in contrast to certain previous studies such as Fang et al. (2013a;
206 2014) and Lee et al. (2012), although in agreement with the conclusions of García et al.
207 (2016).

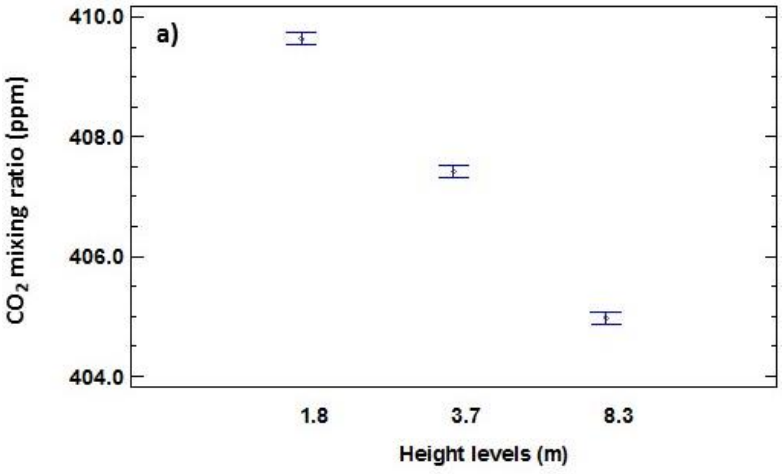

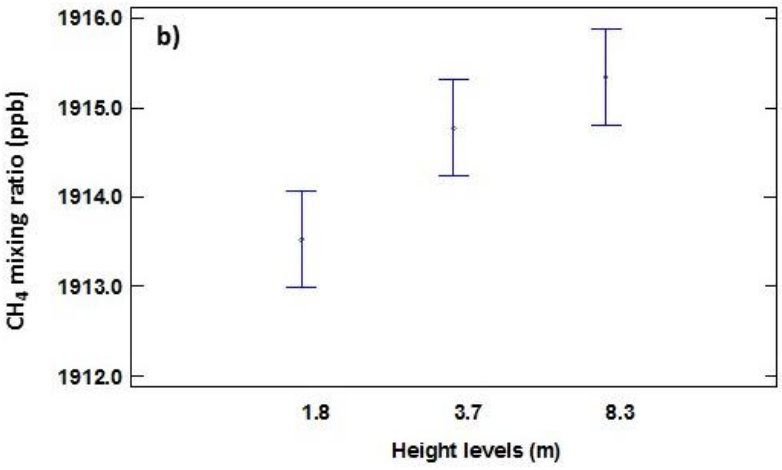

208

209 Fig. 3. Least significant difference (LSD) intervals for CO_2 and CH_4 mixing ratio at
210 night-time for the three levels measured: a) CO_2 results. b) CH_4 results.

211 No strong differences could be inferred between the three height levels (Figs. 2 and 3).
212 The highest (8.3 m) was thus used to describe the CO_2 and CH_4 cycle in the following
213 sections.

214 *3.2. Global evolution*

215 Global evolution of CO_2 and CH_4 have been obtained from Eq (1). The annual average
216 concentration at the CIBA station from 2010 to 2016 was 399.24± 5.05 ppm for CO_2
217 and 1906.63 ± 25.70 ppb for CH_4 during daytime, and 404.83 ± 6.28 ppm (CO_2) and
218 1913.27 ± 24.32 ppb (CH_4) during the night-time. These values were consistent with
219 earlier research in the same study area reported by García et al. (2008). The mean
220 concentrations found for CO_2 closely follow the global values, 394.90 ppm, considering
221 monthly data (NOAA, 2016). CH_4 concentrations at CIBA are higher than global mean
222 values, which represent 1816.49 ppb (NOAA, 2016).

223 Figure 4 depicts the variation of regional CO_2 concentration recorded at the CIBA
224 station. Each box represents the interquartile range where the median is represented by a
225 line. Whiskers extend from the 10^{th} to the 90^{th} percentile. Outliers correspond to the 5^{th}
226 and 95^{th} percentiles.

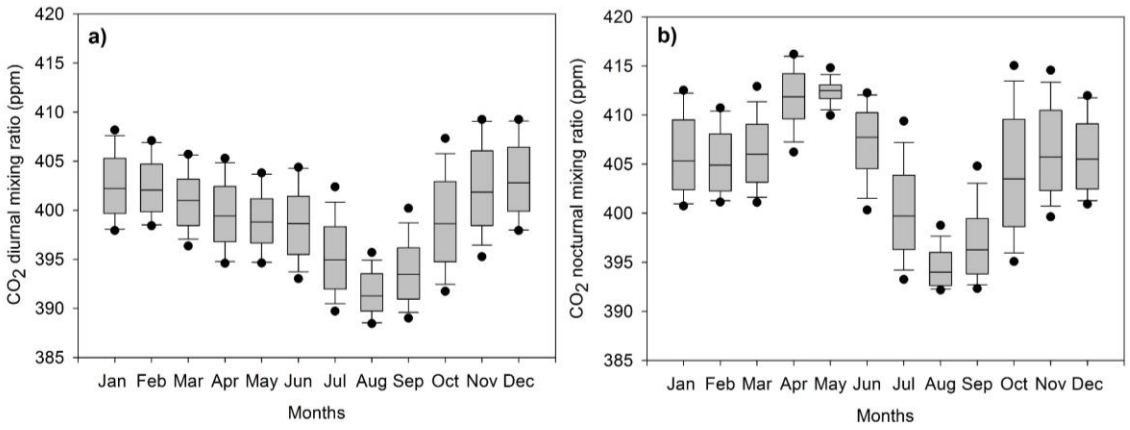

227

228 Fig. 4. Annual evolution of CO_2 measurements over the five and a half years of study at
229 the CIBA station: a) daytime data. b) night-time data.

230 Several points should be noted from Fig. 4. First, it has been evidenced that time of year
231 affects gas concentrations, and second, CO_2 concentrations during the day (Fig. 4a) are
232 higher in winter (maximum in December with 403.17 ppm) and lower in summer
233 (August 391.28 ppm). These results are supported by García et al. (2012). A decreasing
234 pattern from February to August followed by an increase in mean values should be
235 noted.

236 Analyzing CO_2 nocturnal records (Fig. 4b), we detected two peaks as did other
237 researchers such as Sánchez et al. (2010). Sánchez et al. (2010) attributed these
238 temporal variations to strong temperature inversions at the rural site which contributed
239 to trapping CO_2 during night-time especially during the growing season and in autumn
240 (García et al., 2012).

241 The first peak is located in spring (April: 411.72 ppm), corresponding to the period of
242 maximum vegetation growth (Sánchez et al., 2005). In that period, the moisture content
243 of soils and their respiration process play an important role as vegetation becomes
244 photosynthetically active (Lee et al., 2012). Pérez et al. (2009a) have documented the
245 influence of the Valladolid plume over the site in spring, increasing gas concentration.

A decrease in concentration can be observed from May to August. The same behaviour has been explained by García et al. (2008), Pérez et al. (2009a) and Sánchez et al. (2003; 2005). This decrease might be attributed to the lack of vegetation (the harvest season), higher temperatures and low soil moisture, factors that may diminish the respiration process (García et al., 2010). Lower anthropogenic emissions during the summer due to the absence of heating and the reduction in traffic and industrial activities must also be considered (García et al., 2012). The second maximum occurs in autumn (November, 405.74 ppm) as reported by Sánchez et al. (2003). These authors attribute this fact to local soil disturbances caused by ploughing the soil while preparing the land for seeding and to an increase in the amount of precipitations, as also pointed out by García et al. (2008). According to Sun et al. (2014), this peak seems to be linked to increased ecosystem productivity as well as soil microbial activity and respiration processes (Kirschke et al., 2013). Moreover, at this time of the year the Palencia plume has an impact on the site (Pérez et al., 2009a), although its emissions are four times lower than Valladolid emissions (Pérez et al., 2009b). Due to the smaller population of Palencia and the greater distance from the CIBA station, its plume has less of an impact on the measuring point than the Valladolid plume (Pérez et al., 2009b; 2012a).

The nocturnal CO_2 minimum is also located in summer (August 394.01 ppm) as occurs during the daytime, indicating the strong absorption by land biosphere in the middle of the year (Fang et al., 2016). These results are in agreement with the CO_2 cycle in the Northern Hemisphere, which is mainly dominated by photosynthetic activity and which evidences rapid decreases from June to August and large increments from September to December (Fang et al., 2014). Transport processes during night-time described by Pérez et al. (2012b) showed low concentrations of CO_2 associated with the NE, WSW and SSW wind prevalence.

The CH_4 cycle is simpler, showing peaks in winter and troughs in summer (Fig. 5). This pattern is in line with other research in the Northern Hemisphere. Some examples include the conclusions of Fang et al. (2015) and García et al. (2016). The box plots in Fig. 5 illustrate the annual CH_4 cycle. Outliers, as reported by Sánchez et al. (2014), may be attributed to high emissions from Valladolid and Palencia and to the impact of fugitive emissions from a landfill, located near the monitoring station, which releases around 7.11 kt $year^{-1}$ into the atmosphere. The local influence of livestock in the region must also be mentioned. This makes it a major source of CH_4 emissions with approximately 197 kt $year^{-1}$. In line with García et al. (2016), from a long range standpoint, the main pollutant sources come from European trajectories, specifically, in our case from the southeast sector where the urban landfill is located.

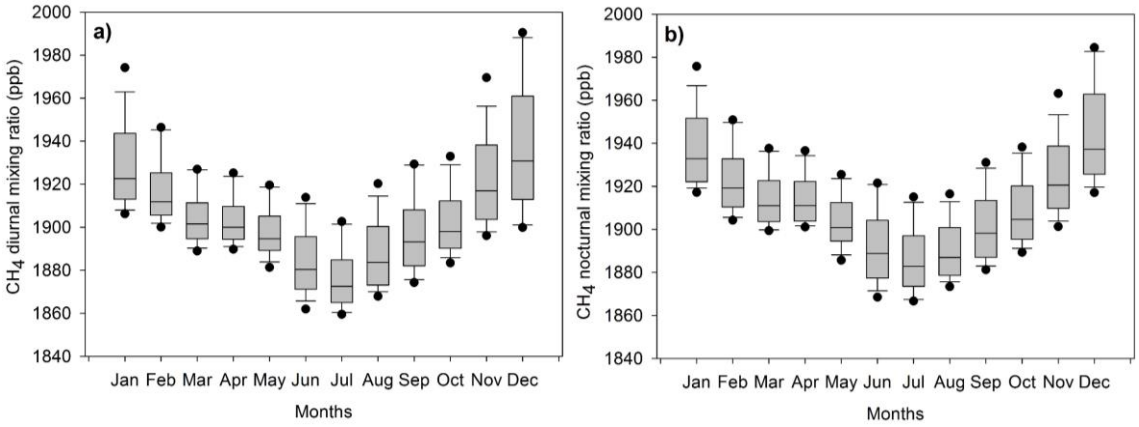

Fig. 5. Annual CH_4 mixing ratio at the CIBA station over the whole study period: a) diurnal measurements. b) nocturnal measurements.

The highest mole fractions occur in December, average 1937.86 ppb during the daytime (Fig. 5a) and 1944.36 ppb during the night-time (Fig. 5b). The low presence of radicals during winter leads to increased CH_4 in this season (Fang et al., 2013a). At the same time, biomass burning begins around October in the upper Spanish plateau and might influence the cycle as Fang et al. (2013a) has suggested for other sites.

The minimum concentration was found in July and was 1877.22 ppb for daytime data and 1886.74 ppb for the nocturnal dataset. The main reason for the minimum point results from the higher temperatures, which dry the croplands, thereby reducing plant activity and increasing CH_4 oxidation, which is considered the principal removal process (García et al., 2016).

Lower mixing ratios of both greenhouse gases in summertime have been detected. Al-Anzi et al. (2016) explain this behaviour because of the higher planetary boundary layer that reinforces pollutant transport and the dispersion process. During this season, solar radiation is also higher, producing good dilution from surface and thus a decrease in CO_2 and CH_4 concentrations (García et al., 2012; Pérez et al., 2009b). The opposite is found for the winter season. Moreover, Atlantic air masses (cleaner masses) are more frequent in summer as are continental air masses (more pollutants) in spring (García et al., 2010).

The CIBA station reveals sharp differences between day and night (Figs. 4 and 5). Higher concentrations at night and lower during the day have been detected in agreement with Martins et al. (2016) and Northern Hemisphere mean values (Pu et al., 2014). These diurnal changes are most marked in the growing season (Pérez et al., 2009c). Newman et al. (2013) found that diurnal variations in CO_2 and CH_4 were mostly influenced by the planetary boundary layer through convection (Sreenivas et al., 2016).

During the daytime, at the CIBA station, the boundary layer extends to a mean of 550 metres (METEX, 2017). Its maximum height in the middle of the day and the stronger vertical mixing (Fang et al., 2014), produce more dilution in the air (García et al., 2016).

313 CO_2 uptake and higher photochemical reactions are also considered important causes of
314 the low CO_2 and CH_4 concentrations (Lee et al., 2012).

315 At night, radiation loss at ground level leads to a shallow stable boundary layer (Fang et
316 al., 2013a) reaching 190 metres at CIBA (METEX, 2017). Atmospheric mixing is low
317 (Haszpra et al., 2008) and turbulent processes decrease. For these reasons, dispersion
318 confines emissions in a narrow mixing layer (García et al., 2012) contributing to trap
319 surface emissions (Fang et al., 2013a). Thermal inversions which are greater at night
320 (Pérez et al., 2009b) and the respiration process also impact on higher concentrations at
321 night (Lee et al., 2012). As regards CH_4, higher concentrations might be explained by
322 the prevalence of easterly and northerly winds in the area at night. Bearing in mind that
323 Palencia is in the northeast, Valladolid in the southeast and the urban landfill in the SSE
324 sector, the highest CH_4 concentrations during night-time are in consonance with the
325 main CH_4 sources in the surrounding area (García et al., 2008; 2016; Sánchez et al.,
326 2014).

327 *3.3. Monthly trend analysis*

328 To study the trend, datasets were deseasonalized in order to analyze only the polynomial
329 term of Eq (1). Monthly mean trend values were then calculated and used to apply
330 simple linear regressions (mixing ratio-time), obtaining the monthly trend equations for
331 CO_2 and CH_4 (Tables 1 and 2). Positive and almost linear trends for CH_4 and CO_2 were
332 found, as reported previously by other researchers such as Buchholz et al. (2016).

333 (Table 1)

334 The outcomes from Table 1 are in consonance with those given by ul-Haq et al. (2017),
335 showing slopes around 2 ppm. The increasing trend is greater in autumn than in spring.

Piao et al. (2008) linked this to higher autumn temperatures caused by climate change, which leads to increased respiration rates (Zhang and Zhou., 2013).

(Table 2)

In the case of CH_4 (Table 2), anthropogenic causes have an impact on autumn and winter emissions.

The satisfactory correlation of the linear fit proves the goodness of the equation. This adjustment was better for CO_2 results. In both cases R^2 was above 0.96.

3.4. Growth rate

According to Barlow et al. (2015), periods of more than a year and a half are good indicators of the growth rate. In this case, a database of five and a half years has been studied.

Figure 6 shows the growth rates of CO_2 and CH_4 which were calculated by the first derivative of trend curves from Eq (1), as other authors, such as Fang et al. (2016), have done previously.

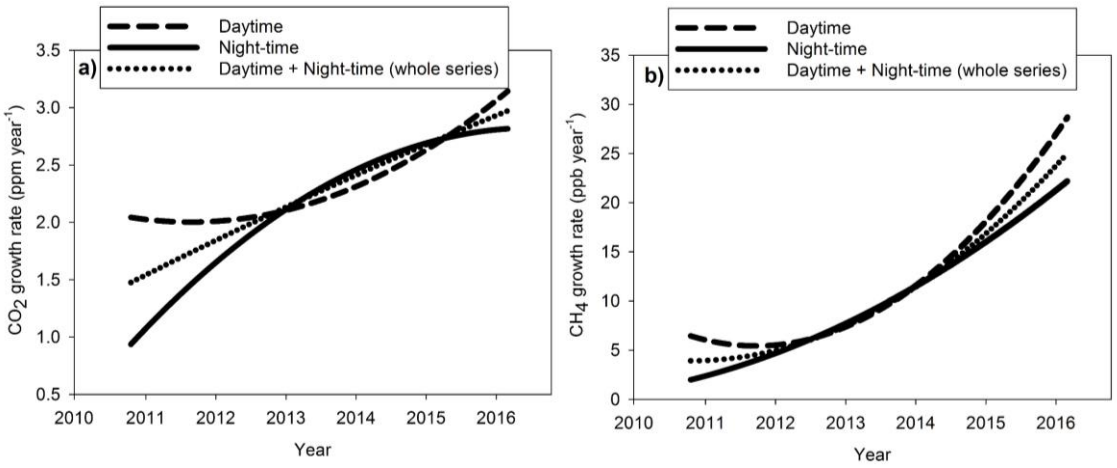

Fig. 6. Growth rates. The dotted line represents the whole data series, the dashed line corresponds to daytime observations, and the continuous line to night-time data a) CO_2 results. b) CH_4 results.

The previous CO_2 results yielded a positive linear increase of 2.32 ppm $year^{-1}$ at the station during daytime conditions, and 2.15 ppm $year^{-1}$ during night-time; with a net growth rate (whole series) of 2.25 ppm $year^{-1}$ (Fig. 6a), slightly higher than the global values of 2.06 ppm $year^{-1}$ for the past decade, (WMO Greenhouse Gas Bulletin, 2015), but lower than those presented by Sánchez et al. (2010) at the same location. These results concur with others shown by García et al. (2010) and Haszpra et al. (2008). The positive CO_2 diurnal growth rate might be derived from vehicle emissions and industrial activities of the nearest cities. The nocturnal increment could be partially attributed to a rise in global mean temperatures over the last five years. This increase may anticipate the beginning of autumn, increasing the respiration rate at nights.

For CH_4 (Fig. 6b), a mean growth rate of 11.90 ppb $year^{-1}$ for diurnal data, and 10.32 ppb $year^{-1}$ for nocturnal outputs has been detected, meaning a net growth rate of 10.95 ppb $year^{-1}$ considering all the data series. These results double Mauna Loa's results (4.7 ppb $year^{-1}$ for the last decade), but are in agreement with those presented by Fang et al. (2016) and Sánchez et al. (2014). The latter author suggested that the contribution of the large amount of livestock in the region may be one reason why the mean growth rate is greater at the CIBA station compared to some non-disturbed areas. Both, daytime and night-time series seem to be mainly influenced by the increase in local anthropogenic emissions from industrial activities, fuel burning and emissions from the urban landfill.

3.5. Seasonal cycle

374 In this section, data were detrended (harmonic data minus polynomial data), working
375 only with the series of harmonics from Eq (1). These are depicted in Fig. 7.

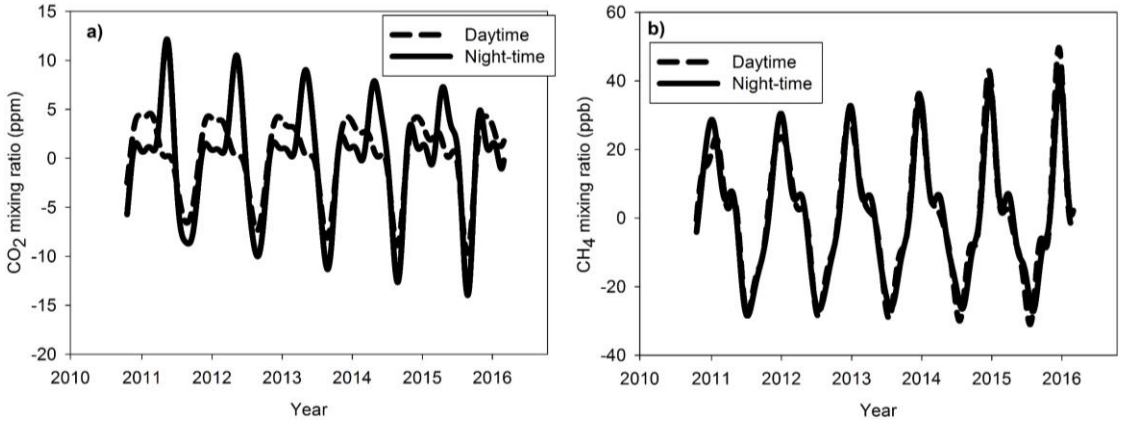

376

377 Fig. 7. Seasonal cycle: a) CO_2 results. b) CH_4 results.

378 The difference between the maximum and minimum value (peak-to-peak) is defined as
379 the amplitude of a cycle. This parameter may be considered as a biological activity
380 indicator (Barlow et al., 2015), but is also influenced by local sources/sinks (Li et al.,
381 2014).

382 CO_2 amplitudes (Fig.7a) were 1.84, 4.59, 6.13 and 2.45 ppm for spring, summer,
383 autumn, and winter, respectively during the day. When analyzing nocturnal series, the
384 results were 7.36, 8.91, 9.97 and 1.59 ppm, respectively. Amplitudes are higher for
385 nocturnal data except in winter due to the greater emissions from heating systems and
386 the lower assimilation rates during cold months.

387 The highest amplitudes were found in autumn, which could be representative of the
388 increase in rainfall during this season as suggested by Buermann et al. (2007). This
389 maximum seems to be in accordance with Lee et al. (2012). The lowest variability was
390 found in spring (daytime) and in winter (night-time). Huang et al. (2015) and Sánchez et

391 al. (2005) have also found lower amplitudes in winter, linking this to the weakest
392 respiratory process by vegetation and roots.

393 An increase in the amplitude of the CO_2 autumnal maximum over night-time data
394 collection was also apparent. These results disagree with those found by Sánchez et al.
395 (2014). Since the amplitude is linked to biological processes (Barlow et al., 2015), this
396 increment could be attributed to an increase in temperatures, stimulating vegetation
397 growth. This leads to an increase in CO_2 emissions through respiration process. This
398 peak occurred earlier over the whole study period in line with the results found by
399 Barlow et al. (2015). The extended growing season caused by higher temperatures in
400 recent years might explain this behaviour in the sampling area. Further studies are
401 needed to confirm such a hypothesis.

402 Seasonal amplitudes for CH_4 (Fig.7b) were 12.90, 12.17, 21.97 and 31.64 ppb during
403 daytime (spring, summer, autumn and winter). For the nocturnal series, results were
404 24.69, 12.69, 17.51 and 22.90 ppb. The highest values in winter (daytime) might be
405 explained by biomass burning. During night-time, maximum values appear in spring
406 and winter, which could be attributed to the strong temperature inversions in these
407 seasons at the CIBA station. The lowest amplitudes occur in summer in both scenarios,
408 which may be associated to photochemical reactions.

409 An increasing trend in seasonal amplitude has been identified in agreement with other
410 observations in the Northern Hemisphere (Sánchez et al., 2010). The annual amplitude
411 growth rate was linear for diurnal values, being 0.7373 ppm (R^2= 0.9995) for CO_2 and
412 5.9 ppb (R^2= 0.9474) for CH_4.

413

414 **4. Conclusions**

415 CO_2 and CH_4 behaviour in the low atmosphere was analyzed in this paper and showed a
416 seasonal pattern from 2010 to 2016. Strong differences were found between day and
417 night-time measurements, with lower values being in evidence during the daytime. The
418 CO_2 cycle revealed sharper differences between day and night compared with the CH_4
419 cycle. During the day, a maximum occurs for CO_2 in December (403.17 ppm) and a
420 minimum in August (391.28 ppm), whereas at night two maximums were observed; the
421 first in April (411.72 ppm) and the second in November (405.74 ppm). The lowest point
422 was also located in August (394.01 ppm). CH_4 peaks were found in December for both
423 scenarios, reaching 1937.86 ppb in daytime conditions, and 1944.36 ppb for night-time.
424 Troughs were found in July, and reached 1877.22 ppb during the daytime and 1886.74
425 ppb during the night. These differences were the result of many factors mainly related
426 with biosphere and biological ecosystem changes (soil humidity, respiration process,
427 amount of precipitations), anthropogenic local sources (plumes, the urban landfill and
428 surrounding agricultural activities) and atmospheric patterns (height of the planetary
429 boundary layer, the prevalence of southeast winds or turbulent processes). Monthly
430 trends led to very stable slopes (around 2 ppm $year^{-1}$ for CO_2 and 10 ppb $year^{-1}$ for CH_4)
431 showing no evidence of stronger effects in certain months. Growth rates were far more
432 accelerated, with higher values than those found at Mauna Loa. Differences were
433 greater during the day (2.32 ppm $year^{-1}$ for CO_2 and 11.90 ppb $year^{-1}$ for CH_4) than
434 during the night (2.15 ppm $year^{-1}$ for CO_2 and 10.32 ppb $year^{-1}$ for CH_4). Seasonal
435 variations due to ecosystem activity and atmospheric behaviour were greater in autumn
436 for CO_2 observations (6.13 ppm for daytime and 9.97 ppm for night-time
437 measurements), in contrast with the CH_4 results that found this maximum during the
438 winter season (31.64 ppb) for the daytime measurements and in spring (24.69 ppb) for
439 the nocturnal data recorded. With all this information, the effectiveness of the harmonic

equation for evaluating temporal trends and seasonal cycles of CO_2 and CH_4 employing a large dataset from a rural area in Southern Europe was demonstrated.

The results obtained might prove useful to understand the processes that govern CO_2 and CH_4 cycles and their future trend, which is essential for designing effective air pollution control and dealing with climate change.

Conflict of interest

The authors declare that there is no conflict of interest regarding publication of this paper.

Acknowledgements

The authors of this paper acknowledge financial support from the Spanish Ministry of Economy and Competitiveness and ERDF funds (projects CGL2009-11979 and CGL2014-53948-P).

References

Al-Anzi, B., Abusam, A., Khan, A.R., 2016. Evaluation of temporal variations in ambient air quality at Jahra using multivariate techniques. *Environmental Technology and Innovation*. 5, 225-232.

Anderson-Cook, C.M., 2000. A second order model for cylindrical data. *Journal of Statistical Computation and Simulation*. 66, 51-65.

Artuso, F., Chamard, P., Piacentino, S., Sferlazzo, D.M., De Silvestri, L., di Sarra, A., Meloni, D., Monteleone, F., 2009. Influence of transport and trends in atmospheric CO_2 at Lampedusa. *Atmospheric Environment*. 43, 3044-3051.

Barlow, J.M., Palmer, P.I., Bruhwiler, L.M., Tans, P., 2015. Analysis of CO_2 mole

462 fraction data: first evidence of large-scale changes in CO_2 uptake at high northern
463 latitudes. *Atmospheric Chemistry and Physics*. 15, 13739-13758.

464 Buchholz, R.R., Paton-Walsh, C., Griffith, D.W.T., Kubistin, D., Caldow, C., Fisher, J.
465 A., Deutscher, N.M., Kettlewell, G., Riggenbach, M., Macatangay, R., Krummel, P.B.,
466 Langenfelds, R.L., 2016. Source and meteorological influences on air quality (CO, CH_4
467 and CO_2) at a Southern Hemisphere urban site. *Atmospheric Environment*. 126, 274-
468 289.

469 Buermann, W., Lintner, B.R., Koven, C.D., Angert, A., Pinzon, J.E., Tucker, C.J., Fung,
470 I.Y., 2007. The changing carbon cycle at Mauna Loa Observatory. *Proceedings of the*
471 *National Academy of Sciences of the United States of America*. 104, 4249-4254.

472 Chamard, P., Thiery, F., di Sarra, A., Ciattaglia, L., De Silvestri, L., Grigioni, P.,
473 Monteleone, F., Piacentino, S., 2003. Interannual variability of atmospheric CO_2 in the
474 Mediterranean: measurements at the island of Lampedusa. *Tellus, Series B: Chemical*
475 *and Physical Meteorology*. 55, 83-93.

476 Fang, S.X., Zhou, L.X., Masarie, K.A., Xu, L., Rella, C.W., 2013a. Study of
477 atmospheric CH_4 mole fractions at three WMO/GAW stations in China. *Journal of*
478 *Geophysical Research: Atmospheres*. 118, 4874-4886.

479 Fang, Z., LingXi, Z., Lin, X., 2013b. Temporal variation of atmospheric CH_4 and the
480 potential source regions at Waliguan, China. *Science China. Earth Sciences.* 56, 727-
481 736.

482 Fang, S.X., Zhou, L.X., Tans, P.P., Ciais, P., Steinbacher, M., Xu, L., Luan, T., 2014. In
483 situ measurement of atmospheric CO_2 at the four WMO/GAW stations in China.
484 *Atmospheric Chemistry and Physics*. 14, 2541-2554.

485 Fang, S.X., Tans, P.P., Steinbacher, M., Zhou, L.X., Luan, T., 2015. Comparison of the
486 regional CO_2 mole fraction filtering approaches at a WMO/GAW regional station in
487 China. A*tmospheric Measurement Techniques*. 8, 5301-5313.

488 Fang, S.X., Tans, P.P., Dong, F., Zhou, H., Luan, T., 2016. Characteristics of
489 atmospheric CO_2 and CH_4 at the Shangdianzi regional background station in China.
490 *Atmospheric Environment*. 131, 1-8.

491 García, M.Á., Sánchez, M.L., Pérez, I.A., De Torre, B., 2008. Continuous carbon
492 dioxide measurements in a rural area in the upper Spanish plateau. *Journal of the Air*
493 *and Waste Management Association*. 58 (7), 940-946.

494 García, M.Á., Sánchez, M.L., Pérez, I.A., 2010. Synoptic weather patterns associated
495 with carbon dioxide levels in Northern Spain. *Science of the Total Environment*. 408,
496 3411-3417.

497 García, M.Á., Sánchez, M.L., Pérez, I.A., 2012. Differences between carbon dioxide
498 levels over suburban and rural sites in Northern Spain. *Environmental Science and*
499 *Pollution Research*. 19, 432-439.

500 García, M.Á., Sánchez, M.L., Pérez, I.A., Ozores, M.I., Pardo, N., 2016. Influence of
501 atmospheric stability and transport on CH_4 concentrations in northern Spain. *Science of*
502 *the Total Environment*. 550, 157-166.

503 Global Carbon Project. 2016. Carbon Budget 2016.
504 http://www.globalcarbonproject.org/carbonbudget/index.htm (accessed 2.16.17).

505 Global Carbon Project. 2016. Methane Budget 2016.
506 http://www.globalcarbonproject.org/methanebudget/index.htm (accessed 2.16.17).

507 Graven, H.D., Keeling, R.F., Piper, S.C., Patra, P.K., Stephens, B.B., Wofsy, S.C.,

508 Welp, L.R., Sweeney, C., Tans, P.P., Kelley, J.J., Daube, B.C., Kort, E.A., Santoni,
509 G.W., Bent, J.D., 2013. Enhanced seasonal exchange of CO_2 by Nothern ecosystems
510 since 1960. *Science*. 341, 1085-1089.

511 Haszpra, L., Barcza, Z., Hidy, D., Szilágyi, I., Dlugokencky, E., Tans, P., 2008. Trends
512 and temporal variations of major greenhouse gases at a rural site in central Europe.
513 *Atmospheric Environment.* 42, 8707-8716.

514 Huang, X., Wang, T., Talbot, R., Xie, M., Mao, H., Li, S., Zhuang, B., Yang, X., Fu, C.,
515 Zhu, C., Zhu, J., Huang, X., Xu, R., 2015. Temporal characteristics of atmospheric CO_2
516 in urban Nanjing, China. *Atmospheric Research*. 153, 437-450.

517 Inoue, H.Y., Matsueda, H., Igarashi, Y., Sawa, Y., Wada, A., Nemoto, K.,Sartorius, H.,
518 Schlosser, C., 2006. Seasonal and Long-Term Variations in Atmospheric CO_2 and ^{85}Kr
519 in Tsukuba, Central Japan. *Journal of the Meteorological Society of Japan*. 84(6), 959-
520 968.

521 Kirschke, S., Bousquet, P., Ciais, P., Saunois, M., Canadell, J.G., Dlugokencky, E.J.,
522 Bergamaschi, P., Bergmann, D., Blake, D.R., Bruhwiler, L., Cameron-Smith, P.,
523 Castaldi, S., Chevallier, F., Feng, L., Fraser, A., Heimann, M., Hodson, E.L.,
524 Houweling, S., Josse, B., Fraser, P.J., Krummel, P.B., Lamarque, J.-F., Langenfelds,
525 R.L., Le Quéré, C., Naik, V., O'Doherty, S., Palmer, P.I., Pison, I., Plummer, D.,
526 Poulter, B., Prinn, R.G., Rigby, M., Ringeval, B., Santini, M., Schmidt, M., Shindell, D.
527 T., Simpson, I.J., Spahni, R., Steele, L.P., Strode, S.A., Sudo, K., Szopa, S., van der
528 Werf, G.R., Voulgarakis, A., Weele, M., Weiss, R.F., Williams, J.E., and Guang, Z.,
529 2013. Three decades of global methane sources and sinks. *Nature Geoscience*. 6, 813-
530 823.

531 Lee, T.R., De Wekker, S.F.J., Andrews, A.E., Kofler, J., Williams, J., 2012. Carbon

532 dioxide variability during cold front passages and fair weather days at a forested
533 mountaintop site. *Atmospheric Environment*. 46, 405-416.

534 Lelieveld, J., 2006. Climate change: a nasty surprise in the greenhouse. *Nature*. 443,
535 405-406.

536 Li, C., Zhou, L., Qin, D., Liu, L., Qin, X., Wang, Z., Ren, J., 2014. Preliminary study of
537 atmospheric carbon dioxide in a glacial area of the Qilian Mountains, west China.
538 *Atmospheric Environment*. 99, 485-490.

539 Liu, M., Wu, J., Zhu, X., He, H., Jia, W., Xiang, W., 2015. Evolution and variation of
540 atmospheric carbon dioxide concentration over terrestrial ecosystems as derived from
541 eddy covariance measurements. *Atmospheric Environment*. 114, 75-82.

542 Martins, C.S.C., Macdonald, C.A., Anderson, I.C., Singh, B.K., 2016. Feedback
543 responses of soil greenhouse gas emissions to climate change are modulated by soil
544 characteristics in dryland ecosystems. *Soil Biology and Biochemistry*. 100, 21-32.

545 METEX (METeorological data EXplorer), 2017.
546 http://db.cger.nies.go.jp/metex/trajectory.html (accessed 1.18.17).

547 Nakazawa, T., Ishizawa, M., Higuchi, K., Trivett, N.B.A., 1997. Two curve fitting
548 methods applied to CO_2 flask data. *Environmetrics*. 8, 197-218.

549 Newman, S., Jeong, S., Fischer, M.L., Xu, X., Haman, C.L., Lefer, B.,Alvarez, S.,
550 Rappenglueck, B., Kort, E.A., Andrews, A.E., Peischl, J., Gurney, K.R., Miller, C.E.,
551 Yung, Y.L., 2013. Diurnal tracking of anthropogenic CO_2 emissions in the Los Angeles
552 basin megacity during spring 2010. *Atmospheric Chemistry and Physics*. 13, 4359-
553 4372.

554 NOAA (National Oceanic and Atmospheric Administration, Global Monitoring
555 Division), 2016. http://www.esrl.noaa.gov/gmd/ (accessed 2.16.17).

556 Pérez, I.A., Sánchez, M.L., García, M.Á., De Torre, B., 2009a. Daily and annual cycle
557 of CO_2 concentration near the surface depending on boundary layer structure at a rural
558 site in Spain. *Theoretical and Applied Climatology*. 98, 269-277.

559 Pérez, I.A., Sánchez, M.L., García, M.Á., De Torre, B., 2009b. CO_2 transport by urban
560 plumes in the upper Spanish plateau. *Science of the Total Environment*. 407, 4934-4938.

561 Pérez, I.A., Sánchez, M.L., García, M.A., De Torre, B., 2009c. Boundary layer structure
562 and stability classification validated with CO_2 concentrations over the Northern Spanish
563 Plateau. *Annales Geophysicae*. 27, 339-349.

564 Pérez, I.A., Sánchez, M.L., García, M.Á., Pardo, N., 2012a. Analysis and fit of surface
565 CO_2 concentrations at a rural site. *Environmental Science and Pollution Research*. 19,
566 3015-3027.

567 Pérez, I.A., Sánchez, M.L., García, M.Á., Pardo, N., 2012b. Spatial analysis of CO_2
568 concentration in an unpolluted environment in northern Spain. *Journal of*
569 *Environmental Management*. 113, 417-425.

570 Pérez, I.A., Sánchez, M.L., García, M.Á., Pardo, N., 2013. Carbon dioxide at an
571 unpolluted site analysed with the smoothing kernel method and skewed distributions.
572 *Science of the Total Environment*. 456-457, 239-245.

573 Pérez, I.A., Sánchez, M.L., García, M.Á., Ozores, M., Pardo, N., 2014. Analysis of
574 carbon dioxide concentration skewness at a rural site. *Science of the Total Environment.*
575 476-477, 158-164.

576 Pérez, I.A., Sánchez, M.L., García, M.Á., Pardo, N., 2016. Features of the annual
577 evolution of CO_2 and CH_4 in the atmosphere of a Mediterranean climate site studied
578 using a nonparametric and a harmonic function. *Atmospheric Pollution Research*. 7,
579 1013-1021.

580 Pérez, I.A., Sánchez, M.L., García, M.Á., Pardo, N., 2017.Trend analysis of CO_2 and
581 CH_4 recorded at a semi-natural site in the northern plateau of the Iberian Peninsula.
582 *Atmospheric Environment.*151, 24-33.

583 Piao, S., Ciais, P., Friedlingstein, P., Peylin, P., Reichstein, M., Luyssaert, S., Margolis,
584 H., Fang, J., Barr, A., Chen, A., Grelle, A., Hollinger, D.Y., Laurila, T., Lindroth, A.,
585 Richardson, A.D., Vesale, T., 2008. Net carbon dioxide losses of northern ecosystem in
586 response to autumn warming. *Nature*. 451, 49-52.

587 Pu, J.J., Xu, H.H., He, J., Fang, S.X., Zhou, L.X., 2014. Estimation of regional
588 background concentration of CO_2 at Lin'an Station in Yangtze River Delta, China.
589 *Atmospheric Environment*. 94, 402-408.

590 Sánchez, M.L., Ozores, M.I., López, M.J., Colle, R., De Torre, B., García, M.A., Pérez,
591 I., 2003. Soil CO_2 fluxes beneath barley on the central Spanish plateau. *Agricultural and*
592 *Forest Meteorology*. 118, 85-95.

593 Sánchez, M.L., García, M.Á., De Torre, B., Pérez, I., 2005. O_3 and CO_2 concentrations
594 in a rural area in central Spain, in: Brebbia, C.A. (Ed.), Air Pollution XIII.WIT
595 Transactions on Ecology and the Environment. UK. 82, 401-410.

596 Sánchez, M.L., García, M.A., Pérez, I.A., de Torre, B., 2008. Evaluation of surface
597 ozone measurements during 2000–2005 at a rural area in the upper Spanish plateau.
598 *Journal of Atmospheric Chemistry*. 60, 137-152.

599 Sánchez, M.L., Pérez, I.A., García, M.A., 2010. Study of CO_2 variability at different
600 temporal scales recorded in a rural Spanish site. *Agricultural and Forest Meteorology*.
601 150, 1168-1173.

602 Sánchez, M.L., García, M.Á., Pérez, I.A., Pardo, N., 2014. CH_4 continuous
603 measurements in the upper Spanish plateau. *Environmental Monitoring and Assessment*.
604 186, 2823-2834.

605 Sreenivas, G., Mahesh, P., Subin, J., Lakshmi, A., Narasimha, P.V., Kumar, V., 2016.
606 Influence of meteorology and interrelationship with greenhouse gases (CO_2 and CH_4) at
607 a suburban site of India. *Atmospheric Chemistry and Physics*. 16, 3953-3967.

608 Sun, Y., Bian, L., Tang, J., Gao, Z., Lu, C., Schnell, R.C., 2014. CO_2 monitoring and
609 background mole fraction at Zhongshan Station, Antarctica. *Atmosphere*. 5, 686-698.

610 Topp, E., Pattey, E., 1997. Soils as sources and sinks for atmospheric methane.
611 *Canadian Journal of Soil Science*. 77, 167-178.

612 ul-Haq, Z., Tariq, S., Ali, M., 2017. Spatiotemporal assessment of CO_2 emissions and
613 its satellite remote sensing over Pakistan and neighboring regions. *Journal of*
614 *Atmospheric and Solar-Terrestrial Physics*. 152-153, 11-19.

615 WMO Greenhouse Gas Bulletin, 2015. The state of greenhouse gases in the atmosphere
616 based on global observations through 2014. World Meteorological Organization.
617 http://www.wmo.int/pages/prog/arep/gaw/ghg/GHGbulletin.html (accessed 12.12.16).

618 Zeng, J., Matsunaga, T., Mukai, H., 2010. METEX-A flexible tool for air trajectory
619 calculation. *Environmental Modelling and Software*. 25, 607-608.

620 Zhang, F., Zhou, L.X., 2013. Implications for CO_2 emissions and sinks changes in
621 western China during 1995-2008 from atmospheric CO_2 at Waliguan. *Tellus, Series B:*

Chemical and Physical Meteorology. 65, 1-14.

Wu, J., Guan, D., Yuan, F., Yang, H., Wang, A., Jin, C., 2012. Evolution of atmospheric carbon dioxide concentration at different temporal scales recorded in a tall forest. *Atmospheric Environment*. 61, 9-14.

Tables

Table 1

Monthly linear regression for CO_2 ($CO_2 = tx + b$) at the CIBA station over the whole study period.

	CO_2 Daytime			**CO_2 Night-time**		
	t (ppm year^{-1})	b (ppm)	R^2	t (ppm year^{-1})	b (ppm)	R^2
January	2.2971	391.22	0.9975	2.2174	397.24	0.9935
February	2.3171	391.33	0.9974	2.2480	397.31	0.9941
March	2.2010	391.80	0.9987	2.1267	397.74	0.9943
April	2.2160	391.93	0.9986	2.1581	397.83	0.9947
May	2.2317	392.07	0.9985	2.1887	397.91	0.9951
June	2.2482	392.22	0.9984	2.2184	397.99	0.9955
July	2.2655	392.36	0.9983	2.2474	398.09	0.9958
August	2.2838	392.50	0.9982	2.2760	398.19	0.9961
September	2.3026	392.63	0.9981	2.3034	398.29	0.9964
October	2.2644	392.99	0.9978	2.1828	398.95	0.9924
November	2.2630	393.21	0.9979	2.1582	399.25	0.9924
December	2.2795	393.36	0.9977	2.1880	399.34	0.9930

t represents the time expressed in years, starting in 2010.

Table 2

Monthly linear regression for CH_4 ($CH_4 = tx + b$) at the CIBA station over the whole study period.

	CH_4 Daytime	**CH_4 Night-time**

	t (ppb year^{-1})	b (ppb)	R^2	t (ppb year^{-1})	b (ppb)	R^2
January	11.3291	1867.59	0.9618	10.3677	1877.48	0.9678
February	11.7308	1867.41	0.9614	10.7056	1877.06	0.9689
March	9.3674	1873.47	0.9752	8.9775	1881.81	0.9749
April	9.6674	1873.45	0.9742	9.2678	1881.66	0.9757
May	9.9839	1873.36	0.9733	9.5630	1881.65	0.9764
June	10.3166	1873.27	0.9726	9.8627	1881.57	0.9771
July	10.6659	1873.36	0.9719	10.1672	1881.37	0.9777
August	11.0376	1873.18	0.9714	10.4816	1881.52	0.9783
September	11.4198	1873.10	0.9710	10.7955	1881.36	0.9790
October	10.7317	1876.72	0.9647	9.9236	1885.78	0.9672
November	10.6401	1878.50	0.9638	9.7580	1887.52	0.9660
December	10.9735	1878.74	0.9627	10.0580	1887.68	0.9669

t represents the time expressed in years, starting in 2010.